Variability in the length of the sea ice season in the middle Eocene Arctic

Catherine E. Stickley[1], Nalân Koç[2,1], Richard B. Pearce[3], Alan E.S. Kemp[3], Richard W. Jordan[4], Francesca Sangiorgi[5] and Kristen St. John[6].

[1]*Department of Geology, University of Tromsø, N-9037 Tromsø, Norway,*

[2]*Norwegian Polar Institute, Polar Environmental Centre, N-9296 Tromsø, Norway,*

[3]*National Oceanography Centre, Southampton, Waterfront Campus, European Way, University of Southampton, Southampton, SO14 3ZH, UK,*

[4]*Department of Earth and Environmental Sciences, Yamagata University, Yamagata 990-8560, Japan,*

[5]*Department of Earth Sciences, Faculty of Geosciences, Laboratory of Palaeobotany and Palynology, Utrecht University, Utrecht, The Netherlands,*

[6]*Department of Geology and Environmental Science, James Madison University, Harrisonburg, Virginia 22807, USA.*

SUPPLEMENTARY INFORMATION

Extended Methods

The BSEI technique lends itself particularly well to very high resolution spatial analysis of laminated diatom-rich sediments on two levels. At low magnifications, porous diatom-rich areas appear dark (low backscatter coefficients), whereas non biogenic, mineral-rich areas (e.g., IRD and pyrite), appear bright (high backscatter coefficients). At higher magnifications the opaline silica of diatom valves and frustules (and other siliceous microfossils) is visible as small bright structures

allowing, with experience, the differentiation of siliceous microfossil groups, genera and even species, in cross-section. BSEI also allows lamination thickness to be measured more accurately than is possible by visual inspection of the core.

At the National Oceanography Centre, Southampton (UK) a core section u-channel was cut into 9 cm sections, sub-sampled cm by cm for topographic SEM imaging and the remaining sample embedded using araldite-based electron microscopy grade resin, prior to sectioning and polishing. An Edwards 306 carbon-coater was utilised to coat the samples with 20 nm of carbon. Scanning electron microscopy (SEM) was undertaken using a LEO 1450VP (variable pressure) instrument. The SEM was operated at 20kV, a working distance of 19-23 mm and a nominal probe current of 750 pA, using both secondary electron (SE) and backscattered electron (BSE) imaging. The BSE detector creates an image, which is a response to the relative atomic mass of the particles and grains. Darker grey material has a relatively light atomic mass (e.g., diatom frustules composed of biogenic silica) and lighter grey/ white grains have a relatively heavy atomic mass (e.g., quartz, pyrite). The elemental composition of the terrigenous fraction was analysed by means of an energy-dispersive X-ray spectroscopy (EDS) PGT (Princeton Gamma Tech) system fitted with a light element detector. SEM BSEI photomosaics taken at x73 and x200 magnification were collected with a 20% field overlap and stitched together using Adobe CS2 software.

Slides were analysed using a Hitachi S-3400N SEM at Statoil ASA (Bergen, Norway). Laminae and sublaminae were logged for composition and sediment fabrics at magnifications up to x1500, using the BSEI photomosaics taken at x73 and x200

magnification for guidance. Siliceous microfossil content, quantity and particle size of terrigenous material, thickness of (sub-)laminae and textural features (grading, sorting, draping, degree of bioturbation and nature of (sub-)laminae boundaries) were noted. Analyses of smear-slides and secondary electron imagery (SEI) of lamina-parallel fracture surfaces aided microfossil identifications. Thickness measurements were undertaken on the x73 photomosaics on-screen using Adobe CS5 software at very high resolution, taking magnification into account at each stage. Rotation of sediment was also taken into account such that lamination thickness was always taken at a 90º angle to the lamination plane.

Age model: Section 5 of Core IODP-302, 55X is at a depth of 240.70 m.c.d. to 241.38 mcd, giving an age of 46.1565 to 46.1846 Ma (i.e., an interval of ca. 28.1 k.y. sedimentation) according to the ACEX age-model (Backman et al., 2008).

Extended Caption for Figure 3 (main text)

Figure 3. Four-stage annual model of production and flux in the middle Eocene Arctic under seasonal sea ice influence. Arbitrary scale.

A. Summer-early autumn. The main (open-water) growing season when insolation is at a maximum as previously described (Stickley et al., 2008). Characterised by flux events of heavily silicified brackish to marine siliceous microfossils such as the diatoms *Anaulus arcticus, Goniothecium danicum, Hemiaulus* spp. and *Stephanopyxis* spp., ebridians and silicoflagellates, and by freshwater chrysophyte cysts. Organic-walled palynomorphs—an important constituent of the middle Eocene Arctic palaeoecosystem (Sangiorgi et al., 2008), are near-impossible to detect using BSEI of polished thin sections. However, since freshwater-tolerant taxa are predominant

during the middle Eocene (Sangiorgi et al., 2008) we assume their reproduction during late spring-summer, followed by encystment and flux during the summer-early autumn period. We therefore assume their predominance in the darker laminations compliant with open water production.

B. Late autumn-winter; sea ice formation and polar darkness. Stock cells of sea ice diatoms are trapped in sea ice forming at the surface and overwinter within the ice. Compare to sea ice-IRD, which is entrained and rafted coastal and shelf sediments. Reconstructed circulation patterns, summarized elsewhere (St. John, 2008), indicate sediment was derived from the Eurasian margin, likely the Kara and Laptev seas. Coastal and shelf sediments are entrained into the sea ice canopy during shore-fast and/or anchor ice formation, and transported offshore. Living *Synedropsis* spp. may also have drifted out to the ridge within sea ice, which formed at the surface some distance from the ridge (although not reworked by shore-fast ice). The extent and coverage of sea ice is unknown in late autumn through early spring (C.). Sea ice thickness is also unknown during the middle Eocene.

C. The early spring sea ice bloom (*Synedropsis* spp.). *Synedropsis* spp. bloom within the bottom ice horizon and/or on the underside of the pack ice above the ridge.

D. Late spring-early summer sea ice melt and break-up. As insolation increases blooming *Synedropsis* spp. are released into the surrounding melt-zone temporarily enriching the surface water, prior to flux to the seafloor. Sea ice-IRD and other terrigenous material are also released at this time.

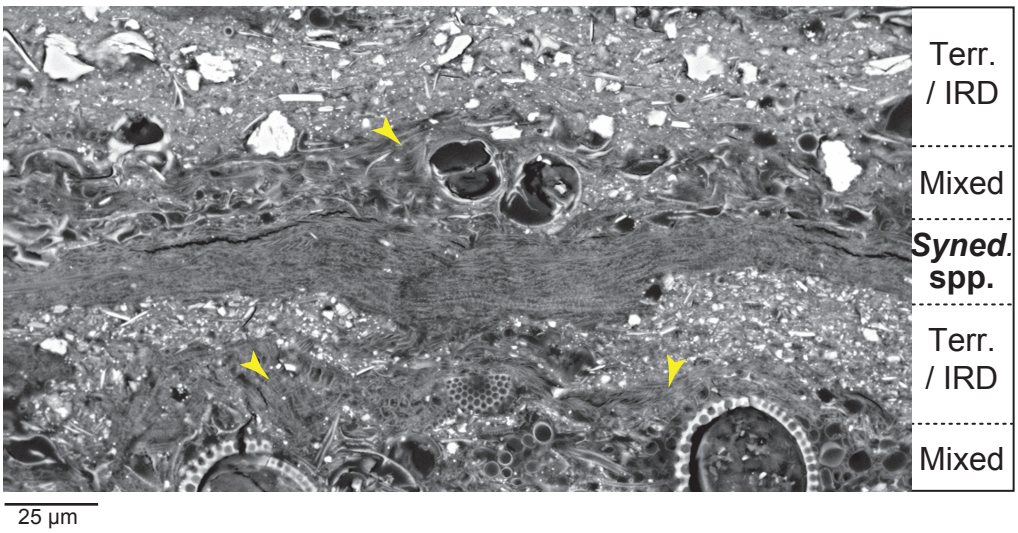

Data Repository Figure 1

SEM BSEI photomosaic close-up of a region of the lower *Synedropsis* spp. lamination (*Syned.* spp) shown in Fig. 2 (main text). Note the lamination appears to be 'fluffy' in texture (a reflection of many frustules comprising the lamination). Isolated blebs of *Synedropsis* spp. frustules are also visible amongst the mixed assemblage laminae (marked by yellow arrows; 3 examples indicated). Terr. / IRD = terrigenous material / IRD. Scale bar = 25 µm. A close-up of *Synedropsis* spp. frustules (from a different area) is proved in Fig. DR2f.

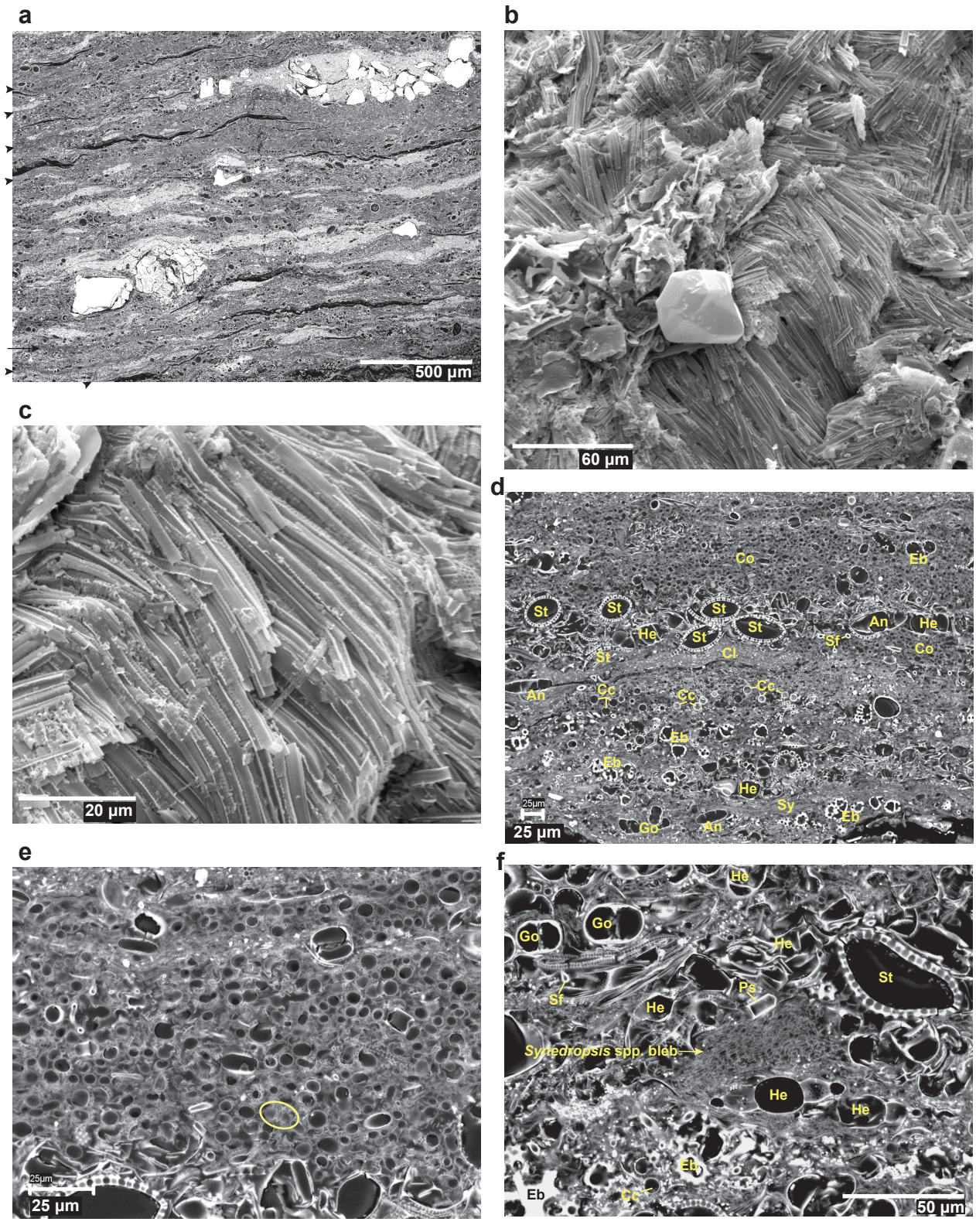

Data Repository Figure 2

Data Repository Figure 2, caption

Close-up scanning electron microscope (SEM) back-scatter electron imagery (BSEI) images and SEM secondary electron (SE) topographic images indicating various features of the microfabric of the study interval. Topographic images are of lamina-parallel fracture surfaces of unprocessed sediment.

a. SEM BSEI image of a part of a typical brighter mm-scale lamina bundle (rich in IRD and *Synedropsis* spp.), showing the wavy nature of the microfabric. The grains and paler microlenses are clay-, silt- and sand-sized terrigenous material (IRD). *Synedropsis* spp. is the dominant siliceous microfossil in this image (individual valves/frustules not visible); a few laminae and micro-lenses of this enigmatic diatom are indicated by the black arrows. Scale bar = 500 μm.

b. SEM SE topographic image of a typical *Synedropsis* spp. lamination indicating how mats of colonies of this diatom typically 'drape' over stronger sedimentary features on the sea-floor during sedimentation to create the wavy microfabric evident in a) (in part). A silt-sized terrigenous grain is prominent in the centre of the image. Scale bar = 60 μm.

c. Close-up of an area of b. Scale bar = 20 μm.

d. SEM BSEI image of a part of a typical darker mm-scale lamina bundle (rich in siliceous microfossils). Definition of the annual cycle using *Synedropsis* spp. laminae is less obvious for the darker mm-scale lamina bundles since sea ice diatoms are in relatively low abundance (see main text). Instead, however, dominant successions of open water taxa are apparent, suggesting that successive productivity-flux events occurred through periods of extended open-water production prior to sea ice reformation. Lamination is clearly evident in this example; the lower half of the image is a mixed assemblage lamination of ebridians (Eb) and chrysophyte cysts (Cc) with minor amounts of the diatoms *Hemiaulus* spp. (He), *Anaulus arcticus* (An), *Goniothecium danicum* (Go) and *Synedropsis* spp. (Sy.). This is overlain by a mixed lamination of the diatoms *Stephanopyxis* spp. (St) and *Hemiaulus* spp. (He). The upper third of the image is an almost monospecific lamination of the small diatom *Costopyxis trochlea* (Co). Silicoflagellates are present throughout the image indicated by the small bright circular to oval features marked in one example (Sf). Cl = clay. Scale bar = 25 μm.

e. Close-up of the *Costopyxis trochlea* lamination indicated in d. Most valves and frustules of this small cylindrical diatom are cut in cross-section, and therefore appear as small rounded structures. A complete frustule of *Costopyxis trochlea* is lying parallel to the plane of the microscope slide (circled). Scale bar = 25 μm.

f. SEM BSEI image of a part of a darker mm-scale lamina bundle containing an isolated bleb of a number of frustules of *Synedropsis* spp. (Sy), indicated in the centre of the image. The typical fluffy appearance of many frustules of this diatom in cross-section is evident. The image as a whole shows the mixed nature of the darker mm-scale lamina bundles. Other siliceous microfossils include ebridians (Eb), chrysophyte cysts (Cc), silicoflagellates (Sf) and the diatoms *Hemiaulus* spp. (He) (at least 2 taxa are present in this image), *Goniothecium danicum* (Go), *Stephanopyxis* spp. (St) and *Pseudopyxilla dubia* (Ps). Scale bar = 50 μm.

Data Repository Table 1a

Lab. slide #	# brighter lamina bundles	# darker lamina bundles	# lamina bundle pairs [#lamina bundle sequences]†	Total thickness laminated sequence(s) (mm)	Total thickness homogenised sediment (mm)	Total thickness disturbed sediment (mm)	Slide length (mm)
P-1A	hard to define	hard to define	0	0.0	10.36	20.30	30.66
P-2A	14	15	7+7 [2] + 1 single darker lam.	27.69	0.0	8.54	36.23
P-3A	6	6	6 [1]	18.92	0.0	12.29	31.20
P-4	12	11	6+5 [2] + 1 single lighter lam.	24.86	0.0	4.71	29.57
P-5	hard to define	hard to define	0	0.0	0.0	28.0	28.00
"P1"	3	3	3 [1]	10.15	0.0	16.37	26.52
"P2"	13	13	13 [1]	25.42	0.0	3.92	29.34
"P3"	4	4	1+1+2 [3]	9.58	14.16	8.42	32.16
P-6	6	6	6 [1]	14.24	0.0	14.81	29.05
P-7	hard to define	hard to define	0	0.0	15.86	13.38	29.24
P-8	8	9	8 [1] + 1 single darker lam.	23.18	0.0	8.12	31.31
P-9	5	5	2+3 [2]	11.38	10.66	5.98	28.02
P-10	4	4	4 [1]	17.69	9.76	3.04	30.50
P-11	11	10	4+6 [2] + 1 single lighter lam.	24.99	4.28	0.0	29.27
P-12	9	9	5+4 [2]	19.48	11.72	0.67	31.88
P-13	7	7	3+2+2 [3]	23.47	4.20	1.08	28.75
P-14	9	9	6+3 [2]	18.16	0.0	7.89	26.05
P-15	14	14	14 [1]	25.67	0.0	0.0	25.67
P-16	hard to define	hard to define	0	0.0	0.0	25.46	25.46
P-17	5	6	5 [1] + 1 single darker lam.	12.56	11.10	0.0	23.66
P-18	hard to define	hard to define	0	0.0	0.0	31.69	31.69
P-19	hard to define	hard to define	0	0.0	14.77	12.21	26.98
P-20	5	4	1+3 [2] + 1 single lighter lam.	11.18	8.99	5.84	26.02
Totals	**135**	**135**	**132 [28]**	**318.61**	**115.87**	**232.74**	**667.22**

Data Repository Table 1a, caption
The number of mm-scale lamina bundles, lamina bundle pairs and lamina bundle sequences noted per slide and in total. Also given are sediment thicknesses for total lamination sequence(s), homogenised and disturbed sediment, per slide and in total. Laboratory slide numbers are arranged in order from top to base of the studied interval. Slide length was measured perpendicular to the lamination or bedding plane on-screen using Adobe Illustrator CS5 that factored in a unique scale for each slide. †see Data Repository Table 2.

Data Repository Table 1b

Total length of sediment processed	**680 mm**
Total length of sediment measured during analysis	**667.22 mm**
Total sediment assumed lost during laboratory processing, or within error limits = 680 - 667.22	**12.78 mm**
Proportion of sediment for which mm-scale lamina bundle sequences can be defined = 318.61 / 667.22 x 100	**47.75%**
Proportion of homogenised sediment = 115.78 / 667.22 x 100	**17.37 %**
Proportion of disturbed sediment = 232.74 / 667.22 x 100	**34.88 %**

Data Repository Table 2

Lab. slide #	Lamina bundle seq. # (top down)	Bundle pair # (top down)	Brighter bundle thickness (mm)	Darker bundle thickness (mm)	Bundle pair thickness (mm)	Sequence thickness (mm)
P-2A	1	1	0.52	0.34	0.86	11.18
		2	0.96	0.50	1.46	
		3	0.15	0.73	0.88	
		4	0.52	0.33	0.86	
		5	0.84	1.41	2.24	
		6	0.90	0.27	1.16	
		7	1.72	2.00	3.72	
	2	1	0.67	4.14	4.81	13.34
		2	0.55	0.34	0.88	
		3	0.54	0.38	0.92	
		4	1.21	0.71	1.92	
		5	1.04	0.49	1.53	
		6	0.29	1.66	1.95	
		7	0.44	0.88	1.32	
	Single bund.	-	-	3.17	-	3.17
P-3A	1	1	0.50	2.86	3.36	18.92
		2	2.32	0.64	2.95	
		3	0.61	0.73	1.35	
		4	2.47	0.67	3.13	
		5	2.42	1.57	3.99	
		6	1.07	3.07	4.14	
P4	1	1	1.12	1.24	2.36	11.19
		2	0.28	0.38	0.66	
		3	0.66	0.50	1.16	
		4	0.84	0.65	1.49	
		5	1.02	0.54	1.57	
		6	3.41	0.54	3.95	
	Single bund.	-	1.54	-	-	1.54
	2	1	1.16	0.57	1.73	12.13
		2	1.10	0.79	1.89	
		3	1.48	0.67	2.15	
		4	2.42	1.57	3.99	
		5	1.40	0.96	2.36	
“P1”	1	1	0.95	1.13	2.08	10.15
		2	2.02	1.48	3.50	
		3	2.66	1.90	4.56	
“P2”	1	1	0.66	0.64	1.30	25.42
		2	0.75	1.00	1.76	
		3	1.10	1.17	2.27	
		4	1.53	0.85	2.39	
		5	1.18	0.61	1.78	
		6	0.72	0.47	1.19	
		7	1.87	1.16	3.03	
		8	0.80	0.58	1.39	
		9	0.52	0.46	0.98	
		10	0.52	0.84	1.36	
		11	0.60	1.52	2.12	
		12	0.71	1.27	1.98	
		13	0.37	3.49	3.87	

Lab. slide #	Lamina bundle seq. # (top down)	Bundle pair # (top down)	Brighter bundle thickness (mm)	Darker bundle thickness (mm)	Bundle pair thickness (mm)	Sequence thickness (mm)
"P3"	1	1	0.69	0.72	1.41	1.41
	2	1	1.55	0.50	2.05	2.05
	3	1	1.25	0.43	1.68	6.12
		2	1.05	3.39	4.44	
P-6	1	1	2.93	0.65	3.58	14.24
		2	0.96	1.31	2.27	
		3	0.86	1.37	2.23	
		4	0.37	0.70	1.06	
		5	1.60	0.76	2.35	
		6	1.84	0.90	2.74	
P-8	1	1	0.89	0.58	1.47	22.59
		2	0.71	0.79	1.49	
		3	1.59	0.75	2.34	
		4	1.43	0.81	2.25	
		5	2.50	0.52	3.02	
		6	2.95	0.97	3.91	
		7	2.26	0.31	2.58	
		8	3.37	2.16	5.53	
	Single bund.	-	-	0.59	-	0.59
P-9	1	1	0.55	0.67	1.22	3.10
		2	1.20	0.67	1.88	
	2	1	1.88	0.70	2.58	8.28
		2	1.32	1.03	2.36	
		3	2.52	0.82	3.35	
P-10	1	1	1.14	1.31	2.44	17.69
		2	3.57	2.30	5.87	
		3	0.72	1.99	2.71	
		4	2.36	4.30	6.66	
P-11	1	1	0.71	0.85	1.56	9.82
		2	1.63	0.60	2.23	
		3	2.50	0.63	3.13	
		4	1.33	1.59	2.91	
	Single bund.	-	2.70	-	-	2.70
	2	1	0.44	0.97	1.41	12.47
		2	0.88	0.68	1.56	
		3	0.50	0.32	0.82	
		4	1.20	0.34	1.54	
		5	2.80	0.76	3.56	
		6	0.60	2.97	3.58	
P-12	1	1	1.03	0.78	1.81	13.44
		2	1.21	0.69	1.90	
		3	1.87	0.90	2.78	
		4	2.34	1.65	3.99	
		5	2.00	0.97	2.96	
	2	1	1.71	0.82	2.53	6.04
		2	1.01	0.46	1.47	
		3	0.60	0.63	1.23	
		4	0.34	0.47	0.81	

Lab. slide #	Lamina bundle seq. # (top down)	Bundle pair # (top down)	Brighter bundle thickness (mm)	Darker bundle thickness (mm)	Bundle pair thickness (mm)	Sequence thickness (mm)
P-13	1	1	2.18	1.69	3.86	9.89
		2	0.70	1.03	1.73	
		3	2.48	1.81	4.30	
	2	1	1.24	0.59	1.82	3.65
		2	1.03	0.80	1.83	
	3	1	6.63	1.46	8.08	9.93
		2	0.44	1.41	1.85	
P-14	1	1	1.98	1.30	3.28	12.32
		2	0.73	0.78	1.51	
		3	0.44	0.51	0.96	
		4	1.87	0.39	2.26	
		5	1.57	0.59	2.17	
		6	0.88	1.16	2.04	
	2	1	1.19	0.93	2.12	5.83
		2	0.76	0.73	1.50	
		3	1.21	1.11	2.32	
P-15	1	1	1.51	1.03	2.54	25.67
		2	1.23	1.15	2.39	
		3	0.33	0.37	0.70	
		4	0.65	0.29	0.95	
		5	0.31	0.40	0.71	
		6	0.44	0.84	1.28	
		7	0.61	0.49	1.09	
		8	0.80	1.52	2.32	
		9	0.46	0.39	0.84	
		10	1.40	1.00	2.40	
		11	1.89	0.66	2.55	
		12	1.64	1.14	2.77	
		13	1.39	1.55	2.94	
		14	0.73	1.46	2.19	
P-17	1	1	1.45	1.57	3.02	9.94
		2	0.85	0.81	1.66	
		3	0.95	0.76	1.72	
		4	0.67	0.81	1.48	
		5	0.97	1.09	2.06	
	Single bund.	-	-	2.62	-	2.62
P-20	1	1	1.33	1.16	2.49	2.49
	Single bund.	-	1.32	-	-	1.32
	2	1	2.06	1.48	3.54	7.37
		2	1.21	0.90	2.11	
		3	0.83	0.89	1.72	

Data Repository Table 2, caption

Details of lamina bundle sequences defined for the studied interval, including thickness values for each type of bundle, bundle pairs and for discrete sequences. Laboratory slide numbers are arranged in order from top to base of the studied interval. Measurements were taken perpendicular to the lamination or bedding plane on-screen using Adobe Illustrator CS5 that factored in a unique scale for each slide.

We confidently identify 270 mm-scale lamina bundles (135 brighter-tone or terrigenous-rich; 135 darker-tone or terrigenous-poor) via BSEI throughout the study interval in 28 isolated sequences that range in thickness from ~1 mm to ~25.7 mm, and that involve undisturbed sequences of between 1 and 14 lamina bundle pairs (brighter + darker) (Data Repository Tables 1a & 2). We conservatively estimate such lamina-fabric is intact for ~48 % of the study interval, and that a further ~17 % of intact sediment is more homogenized in character. The remaining sediment (~35 %) is heavily fractured through core or laboratory disturbance and is not studied in further detail, but a relic fabric indicates primary mm-scale bedding occurs throughout most (up to 83 %) of the study interval.

Accounting for core disturbance, we estimate the terrigenous-poor (darker) lamina bundles range in thickness between ~0.27 and ~4.30 mm (± 0.01 mm) with unimodal distribution whereby thicknesses of 0.7 mm are significant (accounting for ~33 % of the distribution at ± 0.1 mm error, and ~48% at ± 0.2 mm error). The terrigenous-rich (brighter) lamina bundles vary in thickness between ~0.15 and ~6.63 mm (± 0.01 mm) with more complex distribution that indicate thicknesses in the range ~0.5-1.0 mm are significant at ± 0.2 mm error (Data Repository Table 2, Data Repository Fig. 3).

Data Repository Table 3

		References / comments
Distance from the middle of the Kara Sea to the modern location of the ACEX site	ca. 1400 km	Jakobsson et al., 2008*
Distance from the middle of the Kara Sea to the paleo-location of the ACEX site in the middle Eocene	ca. 700 km, at a conservative estimate	Inferences from O'Regan et al., 2008† The Lomonosov Ridge was rifted from the Barents-Kara shelf in the late Paleocene when seafloor spreading began along the Gakkel Ridge (see O'Regan et al., 2008, for summary). Tectonic reconstructions (Fig. 8 of O'Regan et al., 2008) summarizing the post-rifting phase indicate that by the middle Eocene the palaeo-distance from the Kara Sea shelf to the ACEX site had extended to at least approximately half of the modern distance.
The modern drift speed of ice in the Siberian Laptev Sea	4-5 cm per second	Eicken et al., 1997 (main text). The Transpolar Drift, flowing from the Siberian coast across the North Pole and towards the Fram Strait, is one of two main currents in the Arctic Ocean today that transport sea ice; the other being the clockwise-flowing Beaufort Gyre in the western Arctic.
The modern drift speed of ice in the Fram Strait	5-20 cm per second	Polyak et al., 2010 (main text). The drift speed within the Transpolar Drift increases towards the Fram Strait.
Est. time for shore-fast and/or anchor ice formed at the Laptev or Kara Sea shelf to reach modern location of ACEX site	ca. 80 to 405 days	
Est. time for shore-fast and/or anchor ice formed at the Laptev or Kara Sea shelf to reach the paleo-location of ACEX site in the middle Eocene	ca. 40 to 203 days	

*Jakobsson M., Macnab, R., Mayer, L., Anderson, R., Edwards, M., Hatsky, J., Schenke, H. W. and Johnson, P., 2008, An improved bathymetric portrayal of the Arctic Ocean: Implications for ocean modeling and geological, geophysical and oceanographic analyses, Geophysical Research Letters v. 35, doi:10.1029/2008GL033520.

†O'Regan M., Moran K., Backman J., Jakobsson M., Sangiorgi F., Brinkhuis H., Pockalny, R., Skelton, A., Stickley C.E., Koç¸ N., Brumsack, H-J. and Willard, D., 2008, Mid Cenozoic tectonic and paleoenvironmental setting of the central Arctic Ocean, Paleoceanography, 23, PA1S20, doi:10.1029/2007PA001559.

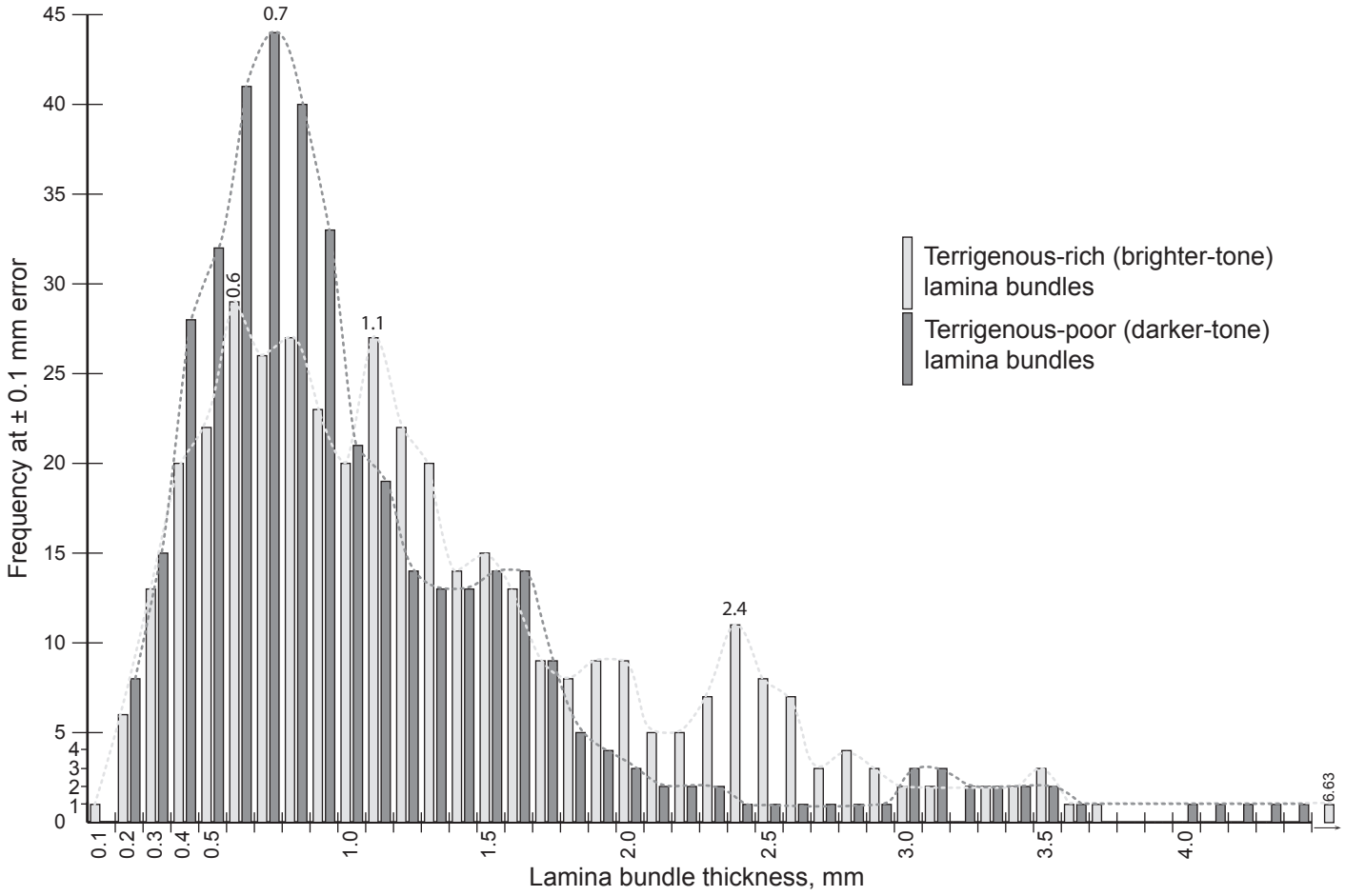

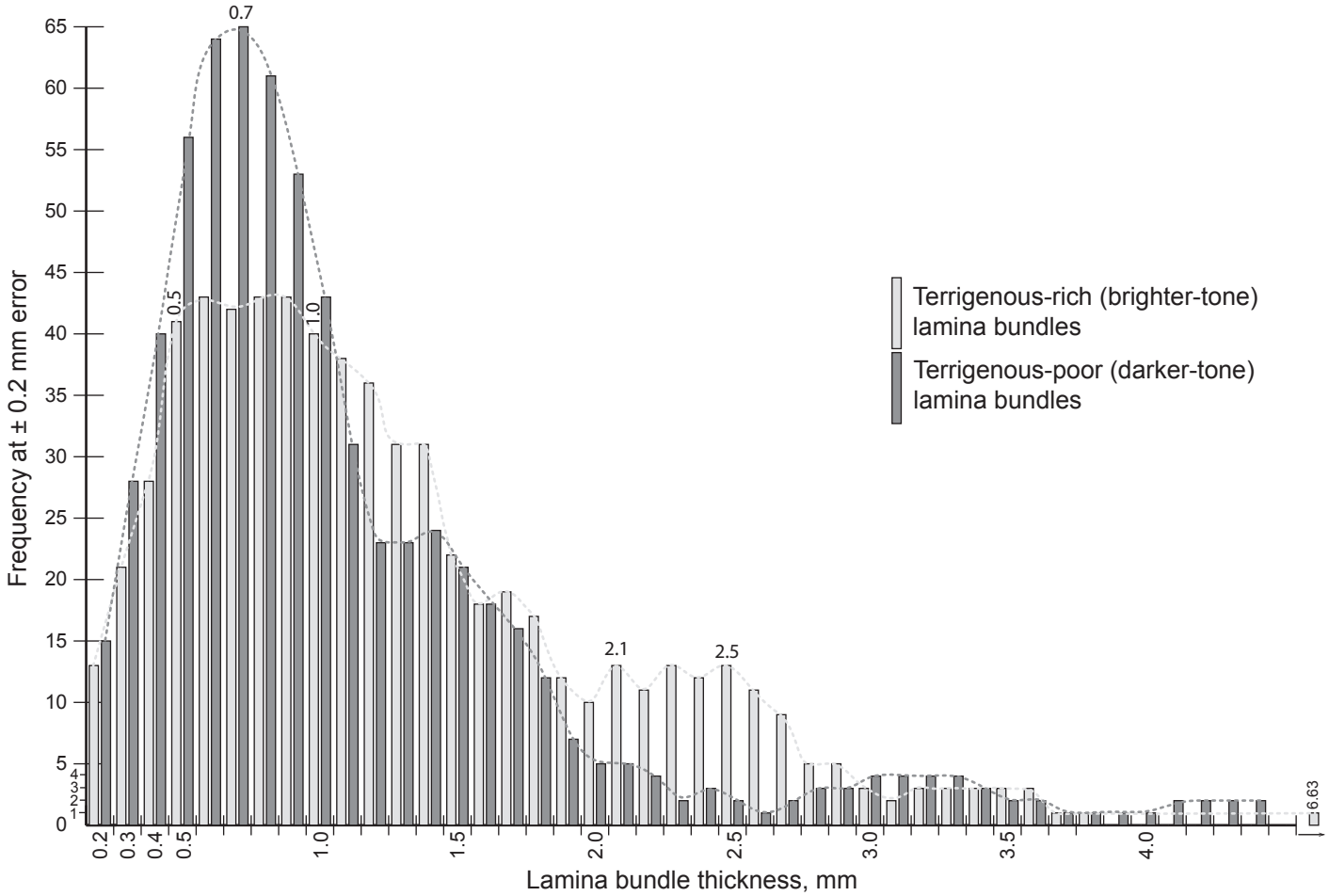

Data Repository Figure 3

Data Repository Figure 3, caption

Frequency distribution for lamina bundle thicknesses in both terrigenous-rich (brighter) and terrigenous-poor (darker) bundle populations at errors of 0.1mm (upper panel) and 0.2 mm (lower panel). Positively skewed unimodal distribution is apparent for each population. The modal thickness value for darker bundles is 0.7 mm at both error estimates, whereas for brighter bundles thicknesses of 0.6 and 1.1 mm are significant at 0.1 mm error, and the thickness range 0.5-1.0 mm is significant at 0.2 mm error. Thicknesses within the 2.1-2.5 mm range may also be significant for brighter bundles.